Structure of Ni(100)-$c(2\times2)$-Na: A LEED analysis

M. M. Nielsen, J. Burchhardt, and D. L. Adams
Institute of Physics and Astronomy, Aarhus University, DK-8000 Aarhus C, Denmark
(Received 15 April 1994; revised manuscript received 17 May 1994)

The structure of Ni(100)-$c(2\times2)$-Na has been investigated by analysis of extensive new low-energy electron-diffraction (LEED) data. The structure is found to contain Na atoms adsorbed in fourfold hollow sites on an unreconstructed and essentially unrelaxed substrate. The Na-Ni layer spacing is 2.38 ± 0.04 Å and the first Ni-Ni layer spacing is 1.75 ± 0.01 Å. These results are in good agreement with the conclusions of an early study by Demuth *et al.* [J. Phys. C **8**, L25 (1975)]. Good agreement between experimental and calculated LEED intensities is obtained using the dynamic theory of LEED, with a conventional, muffin-tin potential for the adsorbed Na atoms and a step potential at the surface. The good agreement pertains not only to the energy positions and relative intensities of peaks in intensity-energy spectra for the diffracted beams, but also to the relative beam intensities, which span a range of nearly two orders of magnitude.

I. INTRODUCTION

The Ni(100)-$c(2\times2)$-Na structure was among the very first overlayer systems to be analyzed by low-energy electron diffraction (LEED). Andersson and Pendry[1] reported in 1972 that Na atoms adsorb in fourfold hollow sites at a distance of 2.87 Å from the first Ni layer. The location of Na atoms was confirmed a few years later by Demuth, Jepsen, and Marcus,[2] but the Na-Ni layer spacing was found to be 2.23 ± 0.1 Å, as later confirmed by a new analysis by Andersson and Pendry.[3] This result, and a similar result for the Al(100)-$c(2\times2)$-Na structure,[4] appears to have formed part of the basis for the general assumption that alkali-metal adsorption on metals occurs without reconstruction of the substrate[5] and, further, that at coverages where superstructures of simple periodicity are formed these involve occupation of high-symmetry sites.

Since these early studies, the local bond geometry has been a neglected aspect of the study of alkali-metal adsorption. Recently, however, there has been a resurgence of interest, in part due to experimental and theoretical studies[6–12] on close-packed Al surfaces which have shown that the adsorption of alkali metals at room temperature leads to a strong[13] reconstruction of the Al substrate Weak reconstructions, involving rumpling or buckling of the first substrate layers, have also been reported for Ni(111)-(2×2)-K,[14] Ni(100)-$c(4\times2)$-K,[15] Ru(0001)-(2×2)-Cs,[16] and for the Al(111)-$(\sqrt{3}\times\sqrt{3})R30°$ structures formed by adsorption of K and Rb at low temperature.[8,12] These observations clearly bring into question the results of earlier studies where such possibilities were not considered, and provide the general motivation for the present work. A surface extended x-ray absorption fine-structure (SEXAFS) study[9] has already shown that the Al(100)-$c(2\times2)$-Na structure involves a reconstruction of the substrate, in disagreement with the result of the early LEED study noted above. For the Ni(100)-$c(2\times2)$-Na structure, however, the present work confirms the conclusion of Demuth, Jepsen, and Marcus[2] that Na atoms occupy fourfold hollow sites on an unreconstructed substrate.

A further question of interest in the present work is whether the conventional theory of LEED can be used to treat the scattering from adsorbed alkali-metal atoms. It has been suggested recently[15] that a postulated much worse agreement between experimental and calculated LEED intensities for systems involving adsorbed alkali metals, relative to that usually obtained for other adsorbate systems and clean surfaces, is due to a nonspherical contribution to the scattering potential resulting from a dipole moment on the adsorbed alkali-metal atom. Although this possibility has not been directly investigated in the present work, we note that good agreement between experimental and calculated intensities is obtained here using a conventional muffin-tin treatment of the scattering from adsorbed Na.

In the following, the experimental methods are described in Sec. II. The LEED intensity calculations and data analysis procedures are described in Secs. III and IV, respectively. The results of the analysis of the experimental LEED data are given in Sec. V, and are summarized and discussed in Sec. VI.

II. EXPERIMENTAL PROCEDURES

The measurements were carried out in a μ-metal ultrahigh-vacuum chamber[17] with base pressure of 3×10^{-11} torr. The chamber was equipped with reverse-view LEED optics,[18] which was used both for LEED intensity measurements and for Auger electron spectroscopy (AES) measurements of surface chemical composition. The Ni(100) crystal was mounted on a manipulator with facilities for rotation of the crystal about two orthogonal axes through the nominal crystal position and with a tilt motion of the manipulator shaft about an axis perpendicular to the shaft at the top of the manipulator. The crystal could be heated by electron bombardment. The crystal temperature was measured using a W-5%Re/W-26%Re thermocouple spot welded to the rear of the crys-

tal. The crystal was cleaned by cycles of Ar^+ bombardment at 600 K and annealing to 1050 K.

Sodium was deposited onto the crystal by evaporation from a source manufactured by SAES.[19] The deposition was carried out incrementally, in a total time of a few minutes, until best development of the $c(2\times2)$ LEED pattern was achieved, at which point the coverage of adsorbed Na is assumed to be 0.5 monolayer. The crystal temperature during Na deposition was 320 K. The residual-gas pressure during evaporation was typically $<2\times10^{-10}$ torr. AES measurements taken after deposition and after completion of a set of LEED measurements indicated that surface contamination, which was almost entirely C, was less than 0.05 monolayer, as calibrated by AES measurements for the Ni(100)-$c(2\times2)$-CO structure, assumed to contain one-half monolayer CO.

The LEED intensity measurements were made using a video-LEED system[20] consisting of a light-sensitive video camera[21] with a silicon-intensifier-target (SIT) phototube,[22] a "frame-grabber" adaptor for digitalization of video images of the LEED pattern on the fluorescent screen of the rearview LEED optics, and a 16/12 bit analog-to-digital (AD) adaptor for programming the electron energy and camera gain, and for reading the electron energy and beam current. The two adaptors[23] are installed in a personal computer. Apart from a simple interface between the AD adaptor and the LEED electronics, the system is based on commercial components and is easily upgradable.

A digital image of the LEED pattern with a geometric resolution of 512×512 pixels and an intensity resolution of 8 bits is obtained at each energy. The intensity of a given diffracted beam is obtained from the digital image by summing the pixel intensities in a window centered on the diffraction spot. The window size is typically set at 15×23 pixels. (The pixels have aspect ratio 4:3.) The full width at half maximum (FWHM) of the LEED spot is typically about 5 pixels. Statistical fluctuations of the order of 10% in the individual pixel intensities are largely averaged out by the summation. The position of the window for a given diffraction spot at a given energy is first calculated using a calibration of the magnification of the optical system and frame grabber, then determined by scanning the intensities within the window to find the position of maximum pixel intensity. The window is then recentered on the determined position and the pixel intensities are summed. This procedure provides a completely robust method for tracking the movement of the diffraction spots with energy. The root-mean-square (rms) deviation between the calculated and determined positions is typically 3–4 pixels, mostly due to about 2% geometric distortion in the SIT phototube.[22] The spot intensity is corrected for background, as measured by summing pixel intensities in windows above and below the diffraction spot, and is normalized for the electron beam current and for the Lambert's law variation of the spot intensity with its position on the fluorescent screen. The spot intensity is also corrected for the spatial variation of the camera sensitivity,[22] as calibrated using a 99.5% homogeneous light source.[24] The intensities of an arbitrary number of beams are measured simultaneously (to within the 40 ms digitalization time). Determination of the spot intensities is carried out in real time and requires about 40 ms per beam at a given energy. The transfer of pixel intensities in a spot window from a frame buffer on the frame grabber to the personal computer accounts for the bulk of this time. Acquisition of an image of the LEED pattern at a given energy is carried out in parallel with the processing of the image acquired at the previous energy, using the two frame buffers on the frame grabber.

The main problem with the video-LEED technique in our implementation is the restricted dynamic range resulting from the dark current in the video camera (typically about 5% of the full video signal) and from the 8-bit representation of pixel intensities in the commercial frame grabber. We have discovered that this problem can be largely overcome, at the cost of some increase in measuring time, by continuously changing the optical gain of the system. This is achieved by programming the gain of the video amplifier of the camera at each energy, in a feedback loop, to achieve near-saturation intensity for a chosen diffraction spot. Since changing the gain of the video amplifier leaves the dark current unchanged, this results in a large increase in the signal-to-noise ratio. Setting the optimum gain at each energy in the feedback loop typically requires the acquisition of 2–3 video frames. However, presumably because of lag in the response of the SIT phototube to changing light levels, a delay of about 300 ms between each frame acquisition is necessary to obtain constant response. By saving the values of the optimal gain at each energy, subsequent runs can be carried out much more rapidly. The gain of the video amplifier is calibrated using the homogeneous light source and proves to be an almost linear function of the programming voltage over a range of almost two orders of magnitude.

In principle, the above procedure could be used to achieve an optimal signal-to-noise ratio for each beam at each energy. However, this would require a separate measurement for each beam and thereby increase the total time for the measurement of a set of intensity spectra by a factor equal to the number of beams of interest. In practice, an acceptable signal-to-noise ratio is obtained by dividing the beams into a few sets according to their average intensities, and programming the camera gain to achieve near-saturation intensity for the brightest beam of the set of interest at each energy. Thus, in the present work, measurements for the generally weaker fractional-order beams were carried out immediately before or after the measurements for the substrate beams, at larger gain settings of the video amplifier and with larger incident beam current. The intensity-energy spectra shown later have been normalized for the video gain and are therefore on the same accurately known (but arbitrary) intensity scale.

Intensity-energy spectra were measured at room temperature in the energy range 40–450 eV at normal incidence, $\theta=0°$, for the clean Ni(100) surface, and at $\theta=0°$, $+10°$, and $-10°$ for the $c(2\times2)$-Na structure. The azimuthal angle of the crystal was set at 0°, such that the plane of incidence coincided with a mirror plane of

TABLE I. Experimental data base for clean Ni(100) and Ni(100)-$c(2\times2)$-Na. R (expt-expt) is the R factor for the comparison of the symmetry-equivalent beams.

	(1×1)	$c(2\times2)$-Na		
Angle of incidence	0°	0°	−10°	+10°
Energy range (eV)	50–450	40–450	40–450	40–450
Energy grid (eV)	1	1	1	1
Total number of beams	19	36	26	26
Symmetry-inequivalent integral-order beams	4	4	9	10
Symmetry-inequivalent fractional-order beams	0	3	7	6
R(expt-expt)	0.008	0.012	0.009	0.012

the surface structure. Repetitive measurements of intensity spectra for given hk beams from the same preparation of the surface structure revealed that random errors in the measurements are very small. In all the spectra shown below these errors are reduced to insignificance by averaging ten sets of measurements, followed by smoothing. The incidence angles were set to within ±0.1° by minimizing the R factor (see Sec. IV) for the comparison of intensity-energy spectra for (nominally) symmetry-equivalent beams. The minimum R factors were of order 0.01 (see Table I). A comparison of such spectra for the $c(2\times2)$-Na structure at $\theta=-10°$ is shown in Fig. 1. Since random errors have been virtually removed, the small differences between the spectra are due to systematic errors, probably caused by errors in angle settings, by inhomogeneities in the response of the fluorescent screen, and possibly also by imperfections in the crystal orientation and surface perfection. The discrepancies between spectra recorded for different preparations of the $c(2\times2)$-Na structure were always less than the discrepancies between symmetry-equivalent beams for a given preparation. The spectra shown later are the result of averaging over ten sets of measurements of the individual hk beams, followed by smoothing, followed by averaging the intensities of symmetry-equivalent beams. The experimental data base is summarized in Table I.

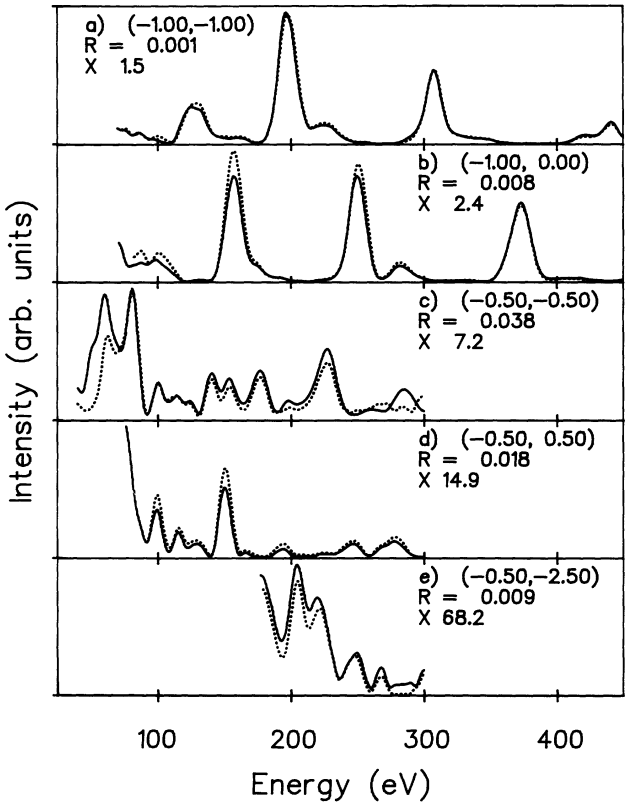

FIG. 1. Comparison of experimental intensity-energy spectra for five pairs (a)–(e) of diffracted beams from the Ni(100)-$c(2\times2)$-Na structure at an incidence angle of $\theta=-10°$. The beams in each pair are nominally equivalent due to mirror-plane symmetry. Each panel shows hk indices for one of the pair of beams, R-factor values for each comparison, calculated via Eq. (4), and scale factors which must be applied to place the spectra for the different beams on the same intensity scale. Note that the peak intensities of this data set span a range of about 70.

III. LEED CALCULATIONS

LEED intensities were calculated using the dynamical theory of LEED, with computer programs derived from the layer-doubling and combined-space programs of Pendry[25] and of Van Hove and Tong.[26] Atomic scattering matrices for Ni and Na were calculated using phase shifts calculated from the muffin-tin band-structure potentials of Moruzzi, Janak, and Williams,[27] and were renormalized for the effects of thermal vibrations using rms isotropic vibrational amplitudes u_{Na} for the adsorbed Na atoms, $u_{\mathrm{Ni},1}$ for the first Ni layer, and $u_{\mathrm{Ni,bulk}}$ for the Ni substrate. Up to 196 partial waves (14 phase shifts) and 139 plane waves (reduced respectively to 24 and 74 symmetry-adapted plane waves at normal incidence and $\theta=\pm10°$) were used, respectively, in the L-space and k-space treatments of multiple scattering within and between layers parallel to the surface. The complex electron self-energy $\Sigma=V_0+iV_{\mathrm{im}}$ was taken to be independent of energy. The surface potential barrier was taken to be a refracting but nonreflecting step of height V_0, positioned at a distance d_{SP} equal to one-half the bulk interlayer spacing above the first layer of atoms.

Refinement of the surface structures of clean Ni(100) and Ni(100)-$c(2\times2)$-Na was carried out using an automatic implementation of a simple, iterative procedure described previously,[28] which makes extensive reuse of scattering matrices, which are stored for all energies, for the individual layers, selvedge, and bulk of the crystal. In each complete iteration, the optimum values of the first

four interlayer spacings d_i and V_0 are determined by minimizing the R factor as a function of each layer spacing in turn for fixed values of the remaining nonstructural parameters $V_{\rm im}$, $u_{\rm Na}$, $u_{\rm Ni,1}$, and $u_{\rm Ni,bulk}$. In each elementary step the optimum value of a particular layer spacing is determined simultaneously with V_0. The procedure was iterated to convergence, which typically required 3–5 passes with the convergence condition that $\sum_{i=0,3}|\Delta d_i| \leq 0.001$ Å, where Δd_i is the change in the optimum value of d_i from one iteration to the next. This took about 15 and 45 min, respectively, for normal incidence and off-normal incidence on a Digital DEC Alpha workstation. The remaining nonstructural parameters and, where appropriate, the interatomic vectors within composite layers, were varied in an outer loop of the refinement, which was also ("manually") iterated to convergence.

IV. R-FACTOR ANALYSIS

The surface structures were determined by minimizing the R factor for the comparison of experimental $I_{hk}^{\rm expt}(E)$ and calculated $I_{hk}^{\rm cal}(E)$ intensity-energy spectra as a function of the structural and nonstructural variables of the calculations defined above. The R factor used here is a normalized χ^2 function defined[28] as

$$R=\sum_{hk,i}\left[\frac{I_{hk,i}^{\rm expt}-cI_{hk,i}^{\rm cal}}{\sigma_{hk,i}}\right]^2\Big/\sum_{hk,i}\left[\frac{I_{hk,i}^{\rm expt}}{\sigma_{hk,i}}\right]^2 , \tag{1}$$

where c is a single, global scaling constant between the experimental and calculated intensities, and $\sigma_{hk,i}$ are the experimental uncertainties at the ith energy point. The scaling constant is determined by the requirement that $\partial R/\partial c=0$ as

$$c=\sum_{hk,i}\left[\frac{I_{hk,i}^{\rm expt}I_{hk,i}^{\rm cal}}{\sigma_{hk,i}^2}\right]\Big/\sum_{hk,i}\left[\frac{I_{hk,i}^{\rm cal}}{\sigma_{hk,i}}\right]^2 . \tag{2}$$

In practice, as noted in Sec. II, it turns out that the values of $\sigma_{hk,i}$ determined from repetitive measurements of experimental spectra are considerably smaller than the discrepancies between symmetry-equivalent beams. Thus to obtain a more realistic measure of the influence of the actual uncertainties we replace the $\sigma_{hk,i}$ by the beam-average rms uncertainties

$$\sigma_{hk}=\frac{1}{n_{hk}}\sum_{i=1}^{n_{hk}}\left[\frac{1}{n_s}\sum_{h'k'}(I_{hk,i}^{\rm expt}-I_{h'k',i}^{\rm expt})^2\right]^{1/2} \tag{3}$$

obtained by comparison of intensities $I_{h'k',i}^{\rm expt}$ for n_s symmetry-equivalent $h'k'$ beams with their average $I_{hk,i}^{\rm expt}$, where n_{hk} is the number of energy points for the beam hk. The R factors for the individual hk beams are defined as

$$r_{hk}=\sum_i (I_{hk,i}^{\rm expt}-cI_{hk,i}^{\rm cal})^2\Big/\sum_i (I_{hk,i}^{\rm expt})^2 . \tag{4}$$

Defining the beam weighting factors

$$w_{hk}=(1/\sigma_{hk}^2)\sum_i (I_{hk,i}^{\rm expt})^2=(1/\sigma_{hk}^2)n_{hk}\langle I_{hk}\rangle^2 , \tag{5}$$

where $\langle I_{hk}\rangle$ is the beam rms intensity, it follows that the total R factor can be written as

$$R=\sum_{hk} w_{hk}r_{hk}\Big/\sum_{hk} w_{hk} . \tag{6}$$

It follows from Eqs. (5) and (6) that, if the ratio $\langle I_{hk}\rangle^2/\sigma_{hk}^2$ is constant, then the contribution r_{hk} of a given hk beam to the total R factor is weighted only by n_{hk} and thus by its energy range. In this event, all beams, strong and weak, contribute to the R factor on an equal footing. In practice, as can be seen from Fig. 2, the ratio is only very roughly constant. Thus the contributions of beams with relatively large errors (with values of σ_{hk} lying above the dashed line in Fig. 2) are downweighted.

In principle, the use of a normalized χ^2 statistic enables estimatation of the uncertainties σ_j in the best-fit values of the calculational variables x_j via

$$\sigma_j^2=2R_{\rm min}/(N_F\partial^2 R/\partial x_j^2) , \tag{7}$$

where $R_{\rm min}$ is the minimum value of the R factor and N_F is the number of degrees of freedom in the fit, and where correlations between the best-fit values have been ignored. In practice, estimates based on this equation yield unrealistically small values for σ_j, presumably because of correlations between the experimental uncertainties which effectively reduce N_F. In order to obtain an objective, if *ad hoc*, estimation of the uncertainties in the best-fit values, we replace the above equation by

$$\sigma_j^2=2kR_{\rm min}/\partial^2 R/\partial x_j^2 , \tag{8}$$

where the constant k is taken to be 0.1. As illustrated later in Fig. 4, this recipe amounts to equating σ_j with the change Δx_j in the optimum value $x_j^{\rm opt}$ corresponding to a 10% increase in R from $R_{\rm min}$.

Finally, it is useful to define[28] the sensitivity s_j of the R factor to the variable x_j as

$$s_j=x_j^{\rm opt}/\sigma_j . \tag{9}$$

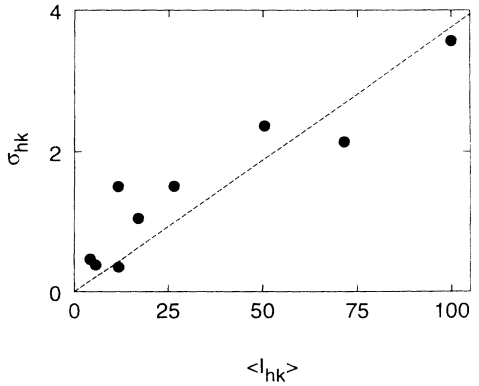

FIG. 2. Plot of the rms uncertainties σ_{hk}, obtained via Eq. (3) as the average over energy of the uncertainties derived from the comparison of nine pairs of nominally equivalent hk beams, as a function of the rms beam intensities $\langle I_{hk}\rangle$, for the experimental intensity spectra at $\theta=-10°$ (see text). The dashed line is a least-squares fit to a straight line through the origin. In constructing the plot the intensities and uncertainties have been scaled with respect to $\langle I_{11}\rangle=100$.

V. RESULTS

A. Clean Ni(100)

The results of the refinement of the structure of clean Ni(100) are shown together with the results for $c(2\times2)$-Na in Table II. As can be seen from the table, the surface structure of Ni(100) corresponds within the experimental error to the truncation of a bulk crystal. However, the vibrational amplitudes of first-layer Ni atoms are found to be about 60% larger than those for deeper layers. A comparison of the experimental intensity-energy spectra with spectra calculated for the optimum parameter values is shown in Fig. 3. The R factor for the comparison is 0.015 as compared to the value of 0.008 for the comparison of the symmetry-equivalent experimental beams.

B. $c(2\times2)$-Na

Preliminary calculations were carried out for structural models involving Na atoms adsorbed in either the onefold on-top sites, fourfold hollow sites, or fourfold substitutional sites consistent with the experimentally observed symmetry. Satisfactory agreement between experimental and calculated intensity spectra was only obtained for adsorption in the fourfold hollow sites. The parameters defining this model were subsequently refined, with results given in Table II. Full refinements were carried out for the data sets at $\theta=0°$, $+10°$, and $-10°$. After completion of the analysis, test calculations were carried out for $\theta=0°$ in which the second Ni layer was split into two layers of $c(2\times2)$ symmetry, with a separation Δr. The R factor was increased by all nonzero values of Δr. Final test calculations were also carried out in which the position of the surface potential barrier, d_{SP}, was varied, together with the interlayer spacings, for fixed, optimum values of the nonstructural parameters. As noted below, the influence of d_{SP} was insignificant.

The relative sensitivity of the R factor to the structural and nonstructural parameters is tabulated in Table III for the analysis of the measurements at $\theta=0°$. It is interesting to note the relatively low value of s_0, the sensitivity to the Na-Ni interlayer spacing, as compared to that for s_1, the sensitivity to the first Ni-Ni interlayer spacing. This result is similar to that found recently for the Al(111)-$(\sqrt{3}\times\sqrt{3})R30°$-Na system.[29] The relative sensitivity of the R factor to the layer spacings d_0 and d_1 and the rms vibrational amplitudes u_{Na}, $u_{Ni,1}$ and $u_{Ni,bulk}$ can also be

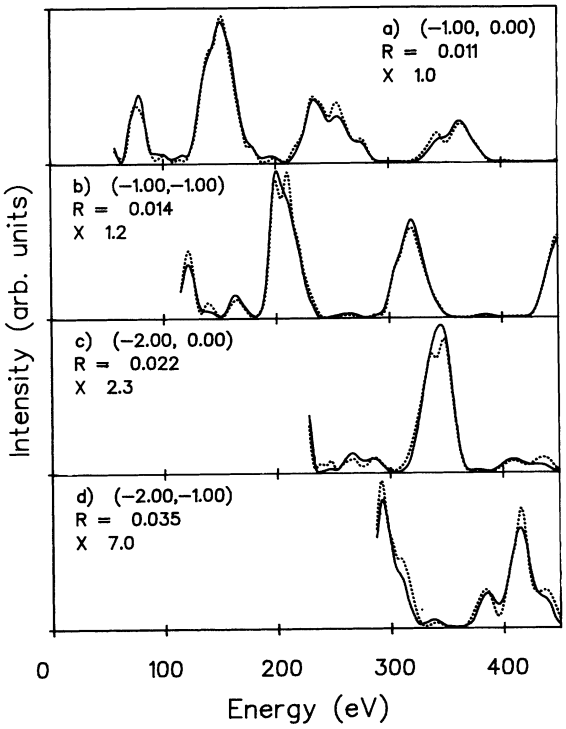

FIG. 3. Comparison of experimental (solid lines) and calculated (dotted lines) intensity-energy spectra for clean Ni(100) at $\theta=0°$ for four diffracted beams (a)–(d). The beam hk indices, R factors, and scale factors are shown in each panel. The calculated spectra were obtained using the best-fit parameter values given in Table II.

TABLE II. Best-fit parameter values for clean Ni(100) and for Na adsorbed in the fourfold hollow site in the Ni(100)-$c(2\times2)$-Na structure. d_i is the ith interlayer spacing. d_0 is the Na-Ni spacing. u_{Na}, $u_{Ni,1}$, and $u_{Ni,bulk}$ are the rms vibrational amplitudes for Na atoms, and for Ni atoms in the first layer and bulk, respectively.

	(1×1)	$c(2\times2)$-Na		
Angle of incidence	0°	0°	−10°	+10°
d_0 (Å)		2.38±0.04	2.38±0.04	2.38±0.04
d_1 (Å)	1.77±0.01	1.74±0.01	1.75±0.01	1.76±0.01
d_2 (Å)	1.76±0.01	1.77±0.01	1.75±0.01	1.76±0.01
d_3 (Å)	1.77±0.01	1.74±0.02	1.75±0.02	1.75±0.01
u_{Na} (Å)		0.25±0.02	0.26±0.02	0.26±0.02
$u_{Ni,1}$ (Å)	0.16±0.02	0.13±0.02	0.12±0.02	0.14±0.02
$u_{Ni,bulk}$ (Å)	0.10±0.01	0.09±0.01	0.10±0.01	0.09±0.01
V_{im} (eV)	3.1±0.6	3.5±0.7	3.7±0.7	3.6±0.5
R	0.015	0.045	0.026	0.042

TABLE III. Sensitivity of the R factor to the structural and nonstructural parameters for the analysis of data taken at $\theta=0°$. [The values are normalized to give $s(d_2)=100$.]

Parameter	d_0	d_1	d_2	d_3	V_{im}	V_0	u_{Na}	$u_{Ni,1}$	$u_{Ni,bulk}$
Sensitivity	48	98	100	71	3.6	8.1	8.4	5.5	6.3

seen in Fig. 4, which contains plots of the R factor as a function of these variables, expressed as percentage changes from their optimum values. The horizontal line in the figure marks a 10% increase in R from its minimum value. As described in Sec. IV, the tabulated errors in the optimum values can be regarded as obtained from the intersection of the curves with this line. (In fact the errors are obtained from Eq. (8) after fitting parabolas to the variation of R with the variables to determine $\partial^2 R/\partial x_j^2$.)

The test calculations in which the R factor was optimized as a function of the position of the surface barrier yielded $d_{SP}=1.05\pm0.7$ Å and a very low sensitivity of $s_{SP}=1.1$. The change in d_{SP} from the value of 0.88 Å used in obtaining the results given in Table II to 1.05 Å led to changes of less than 0.001 Å in the values of d_i.

Comparisons of some of the experimental intensity-energy spectra for $\theta=0°$, $+10°$, and $-10°$ with spectra calculated for the optimum parameter values are shown in Figs. 5–7, respectively. The R factors for the comparisons are 0.045, 0.026, and 0.042, respectively, as compared to the values of 0.012, 0.009, and 0.012 for the comparisons of the sets of symmetry-equivalent experimental beams. As can be seen from the figures, a good level of agreement is achieved between experimental and calculated spectra. We emphasize that this agreement includes not only the peak positions and relative peak intensities for the individual beams, but also the relative hk beam intensities, which span nearly two orders of magnitude for the off-normal incidence measurements. The residual small discrepancies between the experimental and calculated spectra may be due in part to defects in the $c(2\times2)$ structure associated with domain boundaries and/or adsorbed impurities.

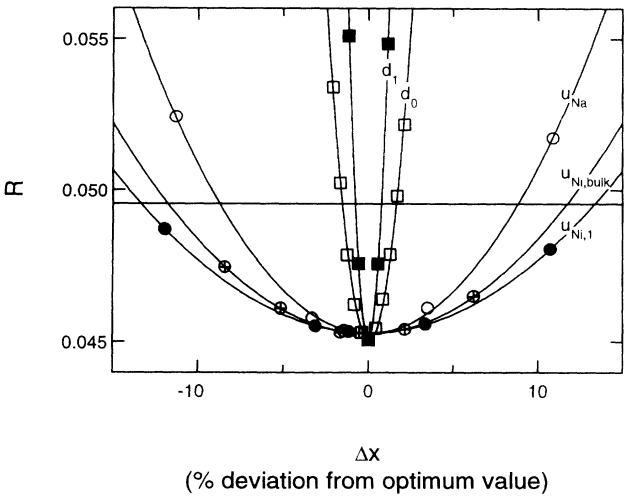

FIG. 4. Plots of the R factor for the comparison of experimental and calculated intensity-energy spectra for Ni(100)-$c(2\times2)$-Na at $\theta=0°$ as a function of the Na-Ni interlayer spacing d_0, the first Ni-Ni interlayer spacing d_1, and the rms vibrational amplitudes u_{Na}, $u_{Ni,1}$, and $u_{Ni,bulk}$ for atoms in the adsorbed Na layer, the first Ni layer, and the Ni substrate. The variables are shown as percentage changes Δx_j from their optimum values x_j^{opt}. The horizontal line in the figure is at $R=1.1R_{min}$, where R_{min} is the minimum value of R. The estimated uncertainties in the best-fit parameter values given in Table II correspond to the values of Δx_j at the intersection of the line at $R=1.1R_{min}$ with the curves in the figure. Note the much larger sensitivity of the R factor to the structural variables (see also Table III). Note also the well-behaved, parabolic variation of R with the variables. (The curves shown are obtained by least-squares fitting of the data points to a second-order polynomial.)

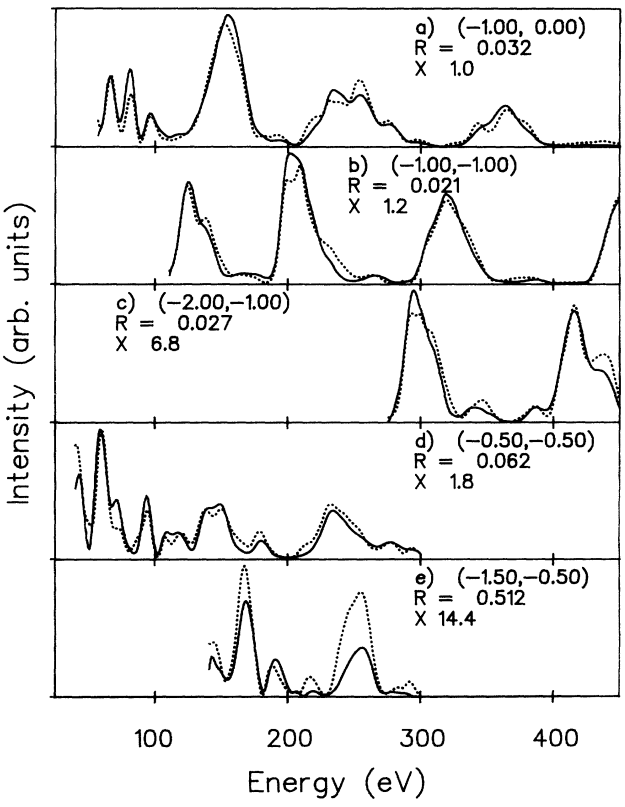

FIG. 5. Comparison of experimental (solid lines) and calculated (dotted lines) intensity-energy spectra for Ni(100)-$c(2\times2)$-Na at $\theta=0°$ for three integral-order beams (a)–(c) and two fractional-order beams (d) and (e). The beam hk indices, R factors, and scale factors are shown in each panel. The calculated spectra were obtained using the best-fit parameter values given in Table II.

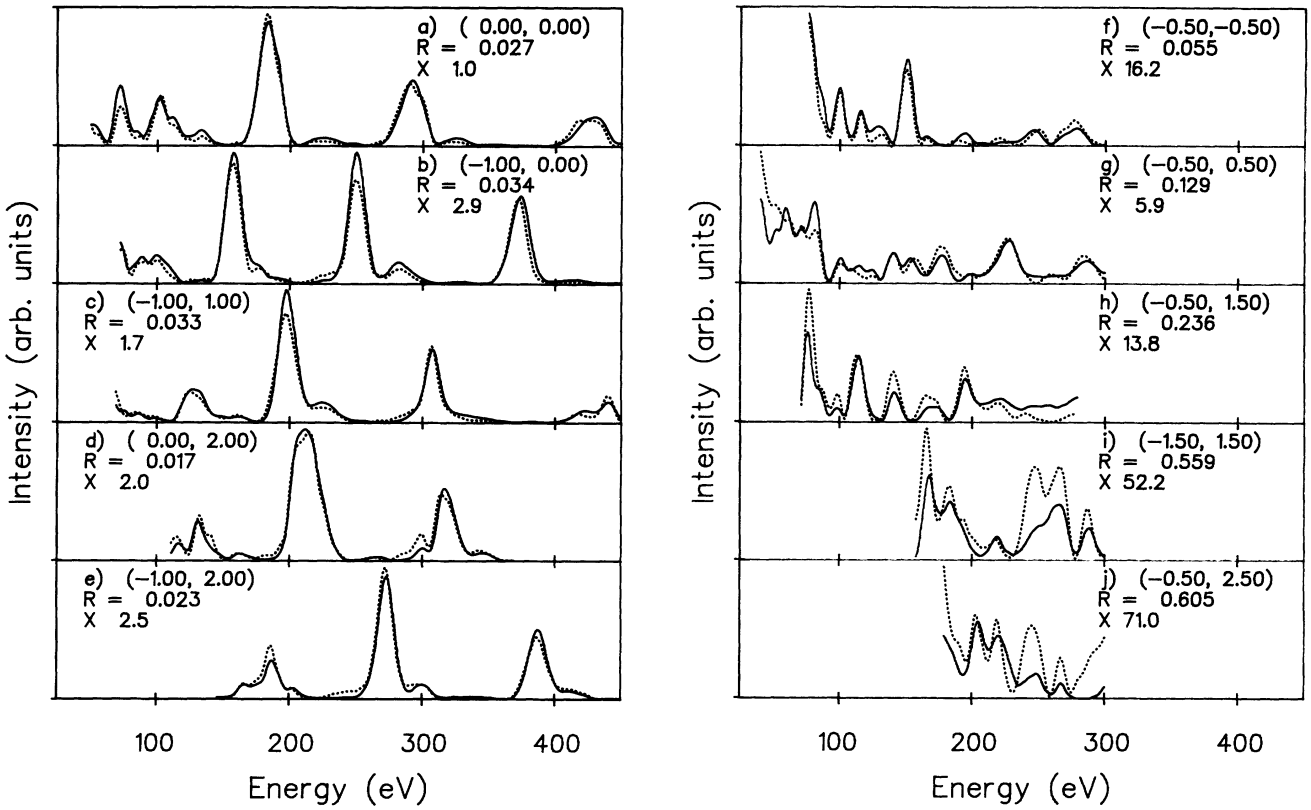

FIG. 6. Comparison of experimental (solid lines) and calculated (dotted lines) intensity-energy spectra for Ni(100)-$c(2\times2)$-Na at $\theta=+10°$ for five integral-order beams (a)–(e) and five fractional-order beams (f)–(j). The beam hk indices, R factors, and scale factors are shown in each panel. The calculated spectra were obtained using the best-fit parameter values given in Table II.

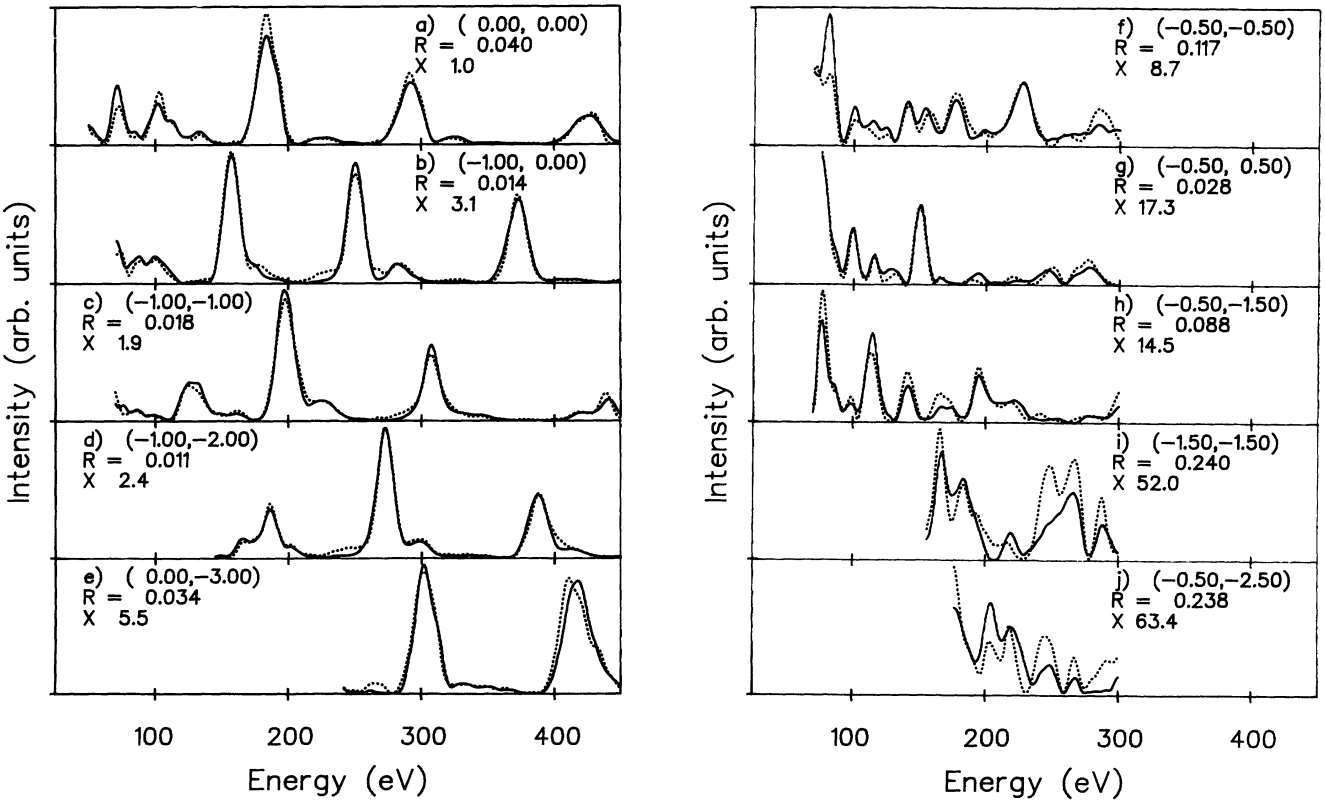

FIG. 7. Comparison of experimental (solid lines) and calculated (dotted lines) intensity-energy spectra for Ni(100)-$c(2\times2)$-Na at $\theta=-10°$ for five integral-order beams (a)–(e) and five fractional-order beams (f)–(j). The beam hk indices, R factors, and scale factors are shown in each panel. The calculated spectra were obtained using the best-fit parameter values given in Table II.

VI. SUMMARY AND DISCUSSION

A. The structures of clean Ni(100) and Ni(100)-$c(2\times2)$-Na

The structure of clean Ni(100) is found to correspond to an almost perfect termination of a bulk crystal, with a first interlayer spacing of 1.77 ± 0.01 Å, as compared to the bulk value of 1.76 Å, in agreement with the conclusions of a number of previous studies.[30–32]

Adsorption of one-half monolayer Na at room temperature yields a $c(2\times2)$ structure in which Na atoms are located in fourfold hollow sites on an unreconstructed and essentially unrelaxed substrate. The Na-Ni interlayer spacing is 2.38 ± 0.04 Å, corresponding to a Na-Ni bond length of 2.95 ± 0.04 Å, and an effective hard-sphere radius of the Na atoms of 1.72 ± 0.04 Å, as compared to the value for bulk Na of 1.86 Å. The first Ni-Ni interlayer spacing is 1.75 ± 0.01 Å. These conclusions are in reasonable agreement with the results of an early study by Demuth, Jepsen, and Marcus,[2] where the Na-Ni interlayer spacing was reported to be 2.23 ± 0.1 Å.

Although we caution that LEED is much less sensitive to nonstructural parameters than to structural parameters, as demonstrated by the results given in Table III and Fig. 3, there is clear evidence from our analysis that the vibrations of Ni atoms in the first layer of the clean surface are about 60% larger than for Ni atoms in deeper layers. These enhanced vibrations are reduced by the adsorption of Na (see Table II). A similar reduction of enhanced vibrations of first-layer Ni atoms on adsorption of K in a $c(2\times4)$ structure has been reported recently by Löffler *et al.*[33] We believe that the inclusion of relative beam intensities in the fitting criterion used here improves the reliability of the determination of vibrational amplitudes.

B. The surface potential

In view of the very approximate description of the surface potential, the question might arise as to how it is possible to obtain good agreement between calculated and experimental LEED intensities over a range of beam intensities of two orders of magnitude. Part of the answer to this question is, of course, that at the energies used here (minimum energy 40 eV) the elastic transmission of the surface potential barrier is very close to unity. The very small sensitivity of the R factor to the position d_{SP} of the potential step, at which the inner potential V_0 and the inelastic damping V_{im} are assumed to set in, is a consequence of the use of a scaling constant [Eq. (2)] between the experimental and calculated intensities. This removes the effect of the attenuation of the amplitude of the incident beam, which occurs on propagation through d_{SP}, and largely removes the effect of the attenuation of the amplitudes of the outgoing beams, for values of the electron energy which are large compared to the damping V_{im}. Sensitivity to the position of the surface barrier and greater sensitivity to V_{im} could obviously be achieved by eliminating the scaling constant. With this in mind, we are currently modifying our experimental procedures with a view to measuring absolute reflectivities.

C. LEED analysis for adsorbed alkali metals

Fritzsche *et al.*[15] have postulated recently that there exists a substantially worse agreement between experimental and calculated LEED intensities for adsorbate systems as compared to clean surfaces, and that this is most extreme when the adsorbate is an alkali metal. They report that for the Ni(100)-$c(4\times2)$-K structure, the agreement, as measured using Pendry's R factor,[34] is improved by inclusion of scattering from a point dipole, which is claimed to compensate for the nonspherical potential caused by a dipole moment on the alkali-metal atom. Since these conclusions have obvious relevance for the present work and a number of other recent studies of alkali-metal adsorption by LEED, we feel obliged to record our doubts regarding their validity.

First, we make the obvious point that measurements on adsorbate systems are inherently less accurate than measurements on clean surfaces. Among a number of extra difficulties, it is evident that a given adsorbate structure can only be perfectly developed, if at all, at a particular coverage. Secondly, we do not accept the postulate that adsorbed alkali metals constitute a worst case as far as agreement between experimental and calculated LEED intensities is concerned. We consider that the level of agreement obtained in the present work and in a number of recent studies[8,12,14,16,29] is at the state of the art and is fairly close to the experimental reproducibility. Thirdly, we do not believe that the necessity to include scattering from a point dipole is firmly established in the work referred to above.[15] We note that the changes in the calculated intensity spectra produced by inclusion of dipole scattering (see Fig. 3 of Ref. 15) are considerably less than the experimental uncertainties (as judged by the differences between the experimental spectra shown in Fig. 2 of Ref. 15 and in Fig. 3 of Ref. 32). Finally, in view of the relative insensitivity of LEED analyses to the nonstructural parameters, it seems evident to us that reliable deductions concerning, for example, atomic scattering properties or thermal vibrations require the use of the full information content of the measurements. Thus the measure of fit should take into account, *inter alia*, the relative peak intensities within the spectrum of a given hk beam, and the relative beam intensities.

ACKNOWLEDGMENTS

The authors would like to thank Klaus Heinz for communication of results prior to publication and for useful discussions. Support of this work by the Danish Natural Science Research Council and Center for Surface Reactivity is gratefully acknowledged.

[1] S. Andersson and J. B. Pendry, J. Phys. C **5**, L41 (1972).

[2] J. E. Demuth, D. W. Jepsen, and P. M. Marcus, J. Phys. C **8**, L25 (1975).

[3] S. Andersson and J. B. Pendry, Solid State Commun. **16**, 563 (1975).

[4] B. A. Hutchins, T. N. Rhodin, and J. E. Demuth, Surf. Sci. **54**, 419 (1976).

[5] Except of course for fcc(110); see R. J. Behm, in *Physics and*

Chemistry of Alkali Metal Adsorption, edited by H. P. Bonzel, A. M. Bradshaw, and G. Ertl (Elsevier, Amsterdam, 1989).

[6]A. Schmalz, S. Aminpirooz, L. Becker, J. Haase, J. Neugebauer, M. Scheffler, D. R. Batchelor, D. L. Adams, and E. Bøgh, Phys. Rev. Lett. **67**, 2163 (1991).

[7]J. Neugebauer and M. Scheffler, Phys. Rev. B **46**, 16 067 (1992).

[8]C. Stampfl, M. Scheffler, H. Over, J. Burchhardt, M. M. Nielsen, D. L. Adams, and W. Moritz, Phys. Rev. Lett. **69**, 1532 (1992); Phys. Rev. B **49**, 4959 (1994).

[9]S. Aminpirooz, A. Schmalz, L. Becker, N. Pangher, J. Haase, M. M. Nielsen, D. R. Batchelor, E. Bøgh, and D. L. Adams, Phys. Rev. B **46**, 15 594 (1992).

[10]J. N. Andersen, M. Qvarford, R. Nyholm, J. F. van Acker, and E. Lundgren, Phys. Rev. Lett. **68**, 94 (1992).

[11]j. N. Andersen, E. Lundgren, R. Nyholm, and M. Qvarford, Surf. Sci. **289**, 307 (1993).

[12]M. M. Nielsen, J. Burchhardt, D. L. Adams, E. Lundgren, and J. N. Andersen, Phys. Rev. Lett. **72**, 3370 (1994).

[13]Here we distinguish *strong* reconstructions in which substrate atoms are removed from their bulk lattice positions, and *weak* reconstructions in which substrate atoms undergo small displacements from their bulk positions. In both cases the resulting structure has a two-dimensional unit cell which is different from that of the corresponding bulk plane.

[14]D. Fisher, S. Chandavarker, I. R. Collins, R. D. Diehl, P. Kaukasoina, and M. Lindroos, Phys. Rev. Lett. **68**, 2786 (1992).

[15]V. Fritzsche, J. B. Pendry, U. Löffler, H. Wedler, M. A. Mendez, and K. Heinz, Surf. Sci. **289**, 389 (1993).

[16]H. Over, H. Bludau, M. Skottke-Klein, G. Ertl, W. Moritz, and C. T. Campbell, Phys. Rev. B **45**, 8638 (1992).

[17]Vacuum Generators Ltd., Hastings, England.

[18]Omicron, Taunusstein, Germany.

[19]SAES Getters, Milan, Italy.

[20]D. L. Adams, S. P. Andersen, and J. Burchhardt, in *The Structure of Surfaces III,* edited by S. Y. Tong, M. A. Van Hove, X. Xide, and K. Takayanagi (Springer, Berlin, 1991), p. 156.

[21]Jørgen Andersen Ingeniør A/S, Copenhagen, Denmark.

[22]RCA data sheet for 4804/H series camera tubes.

[23]Data Translation, Marlboro, Maryland.

[24]Labsphere Inc., North Sutton, New Hampshire.

[25]J. B. Pendry, *Low Energy Electron Diffraction* (Academic, London, 1974).

[26]M. A. Van Hove and S. Y. Tong, *Surface Crystallography by LEED* (Springer-Verlag, Berlin, 1979).

[27]V. L. Moruzzi, J. F. Janak, and A. R. Williams, *Calculated Electronic Properties of Metals* (Pergamon, New York, 1978).

[28]D. L. Adams, V. Jensen, X. F. Sun, and J. H. Vollesen, Phys. Rev. B **38**, 7913 (1988).

[29]J. Burchhardt, M. M. Nielsen, D. L. Adams, E. Lundgren, and J. N. Andersen, Phys. Rev. B **50**, 4718 (1994).

[30]J. E. Demuth, P. M. Marcus, and D. W. Jepsen, Phys. Rev. B **11**, 1460 (1975).

[31]W. Oed, H. Lindner, U. Starke, K. Heinz, and K. Müller, Surf. Sci. **225**, 179 (1989).

[32]U. Muschiol, P. Bayer, K. Heinz, W. Oed, and J. B. Pendry, Suf. Sci. **275**, 185 (1992).

[33]U. Löffler, R. Doll, K. Heinz, and J. B. Pendry, Surf. Sci. (to be published).

[34]J. B. Pendry, J. Phys. C **13**, 937 (1980).